Journal of Applied Physics

Field emission energy distribution and three-terminal current-voltage characteristics from planar graphene edges

Cite as: J. Appl. Phys. **125**, 054502 (2019); https://doi.org/10.1063/1.5064366
Submitted: 03 October 2018 . Accepted: 14 January 2019 . Published Online: 04 February 2019

Jonathan L. Shaw, John B. Boos, Byoung Don Kong, Jeremy T. Robinson, and Glenn G. Jernigan

AIP Publishing

Journal of Applied Physics ARTICLE scitation.org/journal/jap

Field emission energy distribution and three-terminal current-voltage characteristics from planar graphene edges

Cite as: J. Appl. Phys. **125**, 054502 (2019); doi: 10.1063/1.5064366
Submitted: 3 October 2018 · Accepted: 14 January 2019 ·
Published Online: 4 February 2019

Jonathan L. Shaw,[a] John B. Boos,[b] Byoung Don Kong,[c] Jeremy T. Robinson, and Glenn G. Jernigan

AFFILIATIONS

U.S. Naval Research Laboratory, 4555 Overlook Ave SW, Washington, DC 20375, USA

[a]jon.shaw@nrl.navy.mil
[b]KeyW Corp.
[c]**Present address:** Department of Electrical Engineering, Pohang University of Science and Technology (POSTECH), Pohang 37673, Republic of Korea.

ABSTRACT

We demonstrate field emission from an integrated three-terminal device using a suspended planar graphene edge as the source of vacuum electrons. Energy spectra of the emitted electrons confirm the field-emission mechanism. The energy spectra produced by graphene grown by chemical vapor deposition and reduced graphene oxide are compared. The drain-source voltage required to produce a given drain current increases when negative voltages are applied to the gate, confirming field-effect transistor operation. The emission current rises exponentially with inverse voltage over the measured current range from 1 pA to 10 nA. The current-voltage characteristics are consistent with tunneling through barrier potentials calculated numerically from the device geometry.

https://doi.org/10.1063/1.5064366

I. BACKGROUND

Field emission from the suspended edges of graphene fabricated on planar substrates can be used as electron sources for vacuum electronic devices using transport parallel to the substrate surface.[1] Such a quasi-planar architecture, where all electrodes are patterned on a common planar substrate using standard lithography, allows convenient integration and scalability similar to solid state devices. Graphene provides extremely high thermal conductivity, mechanical strength, and chemical stability, which are key requirements for a successful field emission source. Graphene should produce a drain current density roughly 10-100 mA/mm if the emission density achieved from carbon nanotubes applies to graphene and the total current scales with edge length.[2,3] This current level combined with appropriate device design would enable a variety of vacuum electron devices including vacuum transistors which could significantly advance the state-of-the-art in high frequency power performance.

Many field emitter arrays create vertical electron beams originating from sharp tips rising vertically from a planar source substrate.[4] The gate is typically supported on a dielectric film such as silica; good quality thermally grown SiO_2 can sustain at least 100 V/μm without allowing significant current to pass through the bulk or across the surface. Such currents are typically caused by point defects in the material. Energy dissipated by current passing through the dielectric can create additional defects and/or increase the local temperature, possibly leading to dielectric failure (breakdown). If the tip radius is sufficiently small, applying gate-source voltages below the breakdown limit will create an electric field large enough to cause field emission at the apex of the tips. However, there are some longstanding issues with this design: Because the electric field is very sensitive to tip radius, it is difficult to control the tip radius with enough precision to cause uniform emission or to scale the total current with the number of tips (several solutions to this issue are being pursued). Similarly,

reacted and adsorbed material on the emitting area also typically changes the emission current. Finally, the gate-source capacitance stores significant energy. The stored energy reduces the high frequency performance of the device and provides a reservoir of energy that may be dissipated during an arc.

In contrast, planar emission geometries create horizontal electron beams suitable for integrated devices with all electrodes on a single substrate. If implemented on a dielectric substrate, the gate-source capacitance can be dramatically reduced. The use of graphene in an edge geometry as opposed to conventional horizontal tips may improve the emission uniformity and overall linear current density since (a) the thickness of graphene is both very uniform (determined by the carbon atom) and much less than the tunnel barrier thickness (relative thickness changes cause a smaller change in tunneling probability), and (b) graphene does not react with molecular oxygen or most other gases, and adsorbed atoms such as atomic O and F can be removed by heating in vacuum. In addition, graphene is electrically conductive and mechanically strong enough to withstand many times the Coulomb force associated with field emission.[5] The main drawback of the edge geometry is that much lower fields are created at edges versus tips, given the same gate voltage and emitter radius. This issue is partially mitigated by graphene edges because the edge radius of graphene is very small (about 0.15 nm). The electric fields created within the substrate can be reduced by undercutting the graphene edge, and dielectric substrates such as silica or sapphire can typically sustain higher fields than deposited films. Together, these qualities suggest that field emission from planar graphene edges might be used to create integrated vacuum transistors and other devices with all electrodes on a common substrate such that large numbers of devices and circuits could be fabricated using planar lithographic methods.

Several authors have reported field emission from graphene edges to remote electrodes.[6–10] In such cases, large voltages can be applied between the electrodes without causing current due to mechanisms other than field emission. In contrast, when the graphene edge is integrated with an extraction electrode on a common substrate, current can pass through the dielectric materials separating the integrated electrodes. Two-terminal field emission current measured between adjacent integrated graphene edges have been reported by two groups.[11,12] In both reports, the devices were fabricated using graphene transferred onto 300 nm thick SiO_2 layers on conducting silicon substrates. This geometry allows the graphene to be imaged with optical microscopes[13] and provides a way to control the Fermi level in the graphene. However, the large voltages needed to cause field emission create high electric fields throughout the area of oxide supporting the graphene (and its contacts), possibly causing solid state conduction large enough to account for a significant fraction of the measured current. In one report, the lower voltage portion of the I-V curves could be modeled as Frenkel-Poole conduction, supporting the conclusion that transport through the oxide layer did occur.[11] In that case, the functional form of the I-V curve changed from Frenkel-Poole to Fowler-Nordheim above a voltage threshold (no physical effects were measured and only one I-V sweep suggested field emission). Technically, the functional forms of both field emission from graphene and conduction through oxide may not follow the standard Fowler-Nordheim or Frenkel-Poole equations, and the conduction mechanisms can change during the measurement, such that it is difficult to be sure which effects are responsible.[14]

The emission current produced by cold field emission, i.e., tunneling through a barrier potential with unknown shape, created by applying a potential V between the Fermi energies of two electrodes, can generally be described by

$$i(\mathrm{V}) = \mathrm{C}\mathrm{V}^{k} e^{-\mathrm{B}/\mathrm{V}}, \tag{1}$$

where C, B, and k are constants.[15,16] If the emitter is a metal and is not too sharp, the value of k may be close to 2, resulting in the general Fowler-Nordheim form. For emission from a graphene edge, the edge radius is much smaller than the barrier potential thickness and so the classical electrostatic field varies within the barrier potential. This results in a value of k smaller than 2.[17,18] Another complication is that some of the electrons at the graphene edge may be in bound states that cannot be treated as traveling waves [as is assumed in the Wentzel–Kramers–Brillouin (WKB) approximation] and whose concentration may be a function of the emitted current density. Emission from surface states can cause peaks or humps in the emission energy distribution from semiconductors and metals and can result in values of $k < 2$.[19,20] Field emission in the surface normal direction from two-dimensional materials may be affected by quantum confinement that also causes $k < 2$, for example, results indicating $k = 0$ have been reported.[21–23]

To definitively confirm field emission, we built on the earlier reports in several ways: (a) we measured the energy of the emitted electrons, showing that emission to vacuum did occur and that the initial states of the emission were near the Fermi energy; (b) we prepared graphene on bulk dielectric substrates which reduces the maximum electric field in the dielectric, reduces the volume of dielectric where high fields are created during the measurement, and reduces the density of defects; (c) we fabricated a gate electrode between the source and drain electrodes and measured the change in drain current caused by different gate voltages; negative potentials applied to the gate shifted the I_{DS}-V_{DS} curve toward higher V_{DS}. Applying negative voltage to the gate increases the field between the gate and drain, which would increase any solid state transport to the drain. Since the drain current was reduced, the experiment proves that bulk and surface current did not contribute significantly. In addition, we modeled the potential barrier at the graphene edge and confirmed that the current-voltage measurements are in reasonable agreement with the electrostatic model.

II. DEVICE DESIGN AND FABRICATION

We fabricated devices with similar geometry using two different types of graphene: graphene grown by chemical vapor deposition (CVD) and reduced graphene oxide (RGO).

The growth process employed for the CVD graphene resulted in high quality single layer graphene with crystal grains 50-100 μm wide.[24,25] Device fabrication started by transferring the graphene onto a fused silica substrate, using polymethyl methacrylate (PMMA) to support the graphene while the Cu foil is removed by wet etching. Soaking the transferred film in acetone removed the bulk PMMA and drying at 400 °C in forming gas removed most of the residues. Deposition of 20 nm SiO_2 by e-beam evaporation prevented contact with photoresist during subsequent processing steps. Contact lithography followed by etching with buffered hydrofluoric acid and oxygen plasma defined mesas in the graphene. A second lithography step followed by Ti/Au deposition created ohmic contacts at each end of the graphene strip mesas (the source and drain). Source-drain resistance measurements at this point were below 1 kΩ, and Raman spectra verified that the single layer graphene remained intact within the mesa, as shown in Fig. 1. To create the gate, e-beam lithography defined openings in resist approximately 500 nm wide between the source and drain together with contact pads on both sides of the narrow strip. A plasma etch ($CF_4/O_2/Ar$) removed the exposed SiO_2 and graphene, and then exposure to hydrofluoric acid (HF) vapor removed several hundred nm of the exposed silica substrate, undercutting the graphene edges. A Ti/Au deposition formed a gate electrode at the bottom of the resulting trench, self-aligned between the graphene edges. Soaking in acetone followed by critical point drying from isopropyl alcohol removed the resist while avoiding surface tension that might cause the graphene to adhere to the substrate.

Figure 1(a) shows a cross section rendering of a finished device made from CVD graphene on fused silica; Fig. 1(c) shows an optical plan-view image. The gate metal is at the bottom of the trench, self-aligned below the source-drain gap. Based on the optical image, the gate length is roughly 500 nm. The undercut and trench depth are also approximately 500 nm. A Raman system built in-house using a 488 nm laser produced the spectra shown in Fig. 1(d). The spectra shown are an average of several spectra measured over the exposed graphene between the source and drain contacts; one spectrum measured from a device where the graphene was not etched and one from an area that included a cut. The intact graphene [bottom/red spectrum in Fig. 1(d)] shows an intense 2D peak and D/G peak ratio of approximately 0.15, indicating the graphene has high crystalline quality. The Raman spectra averaged over an area including the etched/removed graphene (top/blue spectrum) shows a much larger D peak and D/G ratio of approximately 1, consistent with the expected dangling bonds at the graphene edges. A Raman map of a gated device acquired using a Thermo-Fisher DXR2 SmartRaman Spectrometer using a 532 nm laser is shown in Fig. 1(e). The map shows the integrated G peak area as color, giving confirmation that graphene is present in the intended area.

A second set of devices made with RGO used sapphire substrates coated with 400 nm of germanium but were otherwise

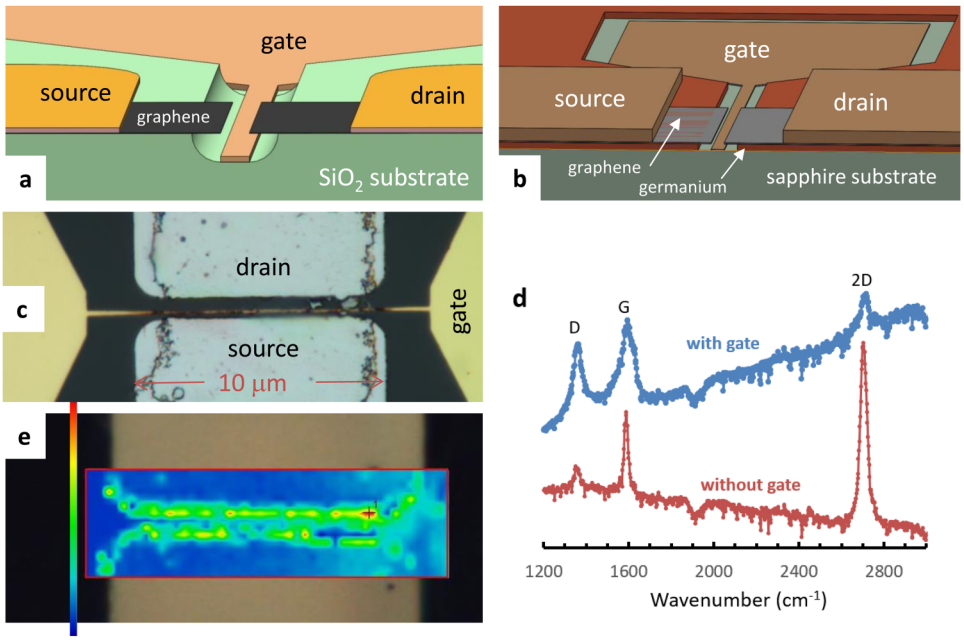

FIG. 1. (a) 3D illustration of device design used for the CVD graphene. (b) Device design used for the RGO. (c) Optical image of the CVD graphene. (d) Raman spectra of the CVD graphene device, averaged over a pristine area (bottom/red) and over an area surrounding the etched line forming the emitter edge. (e) Raman color map superimposed over optical image of a completed CVD graphene device. Most of the graphene is covered with metal. The color bar indicates the intensity of the G peak.

similar to the devices made with CVD graphene. Figure 1(b) is an illustration of the device geometry. RGO preparation was similar to an earlier report.[26] Approximately 2-3 layers of graphene oxide remained after spinning slurry containing dispersed single layer graphene oxide onto the germanium-coated substrate. Annealing the coated wafer at 750 °C in ultra-high vacuum (UHV) caused the oxygen to desorb from the graphene, forming RGO. Much of the conductivity of graphene is recovered by the reduction process; the prepared films showed resistance near 1 kΩ, similar to the CVD graphene. Raman spectra showed an intenseDpeak indicating a large defect density as is typical for RGO. Electron-beam evaporation of 20 nm of SiO_2 protected the RGO from organic materials used later in the process. Contact lithography followed by plasma etching created graphene islands. A second lithography step followed by an HF dip and Ti/Pd deposition and liftoff created source and drain contacts. E-beam lithography defined 500 nm wide openings in resist, and then SF_6 plasma etched the SiO_2-coated graphene and underlying germanium where the resist was removed. E-beam deposition of 80 nm Ti/Pd followed by resist liftoff produced the gates with the top surface 320 nm directly below the graphene edges. Exposure to XeF_2 vapor removed the exposed germanium to undercut the graphene, and then exposure to HF vapor removed the SiO_2 coating from the graphene. We heated the finished devices in UHV in order to remove adsorbed molecules such as fluorine.

III. FIELD EMISSION ENERGY ANALYSIS AND SIMULATION

An elastic tunneling process does not change the electron energies from their initial states and so provides a means to distinguish field emission from other types of vacuum emission. The field emission spectrum is primarily the product of the density of initial state electrons and their tunneling probability versus energy. Therefore, field emission produces electrons near the Fermi energy of the source, in contrast to processes like thermionic emission or photoemission which produce electrons with a minimum energy near the source work function φ_s. Thus, if an unknown emission process produces electrons at energies near the Fermi energy, the emission process can be said to be field emission without regard to the current-voltage response.

The energy-distance diagram in Fig. 2 illustrates the barrier potential and other relevant quantities specific to graphene. The blue shaded area represents the tunneling barrier as seen by an electron at the energy indicated by the blue horizontal arrow. The upper bound of the tunneling barrier is the vacuum potential $U(x)$; the lower bound is the initial energy of the electron. To make the barrier finite, the potential V_{DS} applied to the drain (or other extraction electrodes) with respect to the source must be greater than the work function of the extraction electrode, typically near 4.5 eV. Thus, any current recorded at voltages less than φ_D/e cannot be caused by cold field emission. $U(x)$ is shown as a blue dashed curve assuming an abrupt interface. Since graphene is

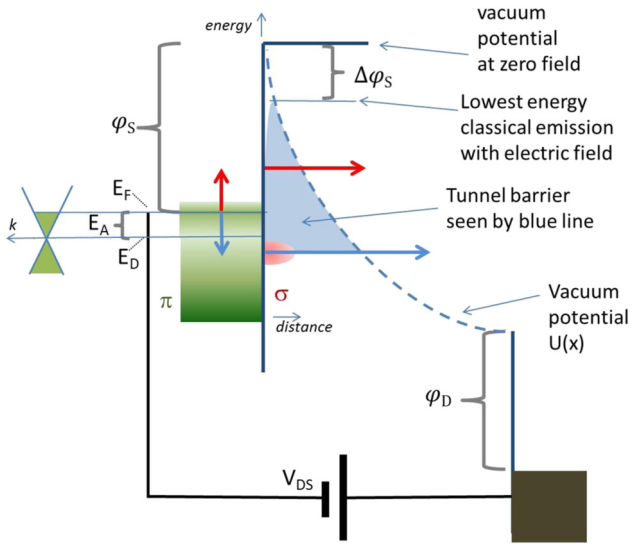

FIG. 2. Illustration of the tunneling barrier potential and graphene initial states.

much thinner than the barrier, the electric field $F(x) = dU(x)/dx$ drops significantly within the barrier. Thus, the tunnel barrier cannot be described as a function of a constant field. Interface effects are expected to reduce $U(x)$ near the graphene edge less than the image charge approximation would suggest (the image charge assumes a planar interface).[17,18,27]

The density of states of semi-infinite graphene (not close to an edge) is linear in energy, as illustrated on the left side of Fig. 2. The energy where the density goes to zero is the Dirac energy E_D. The mobile electrons reside in π orbitals and are delocalized over many atoms. The atoms at an ideal graphene edge can be arranged in armchair and zigzag patterns. The armchair pattern does not contain edge states, whereas the zigzag pattern creates edge states near the Dirac energy.[28] If no edge states were present, the electron density needed to terminate the electric field would be distributed over an accumulated region within a few nm of the edge. The Fermi energy at the edge would need to be near 0.5 eV above the Dirac point, i.e., the graphene bands would bend down at the edge, reducing the work function and increasing the probability of emission. If the edge states and delocalized states react to the electric field in the same way, emission from the armchair regions (free of edge states) would dominate over the zigzag portions where the large edge density would prevent accumulation.[29] However, dangling σ bonds at the edges will be distorted by an electric field due to their parallel alignment, whereas the π orbitals oriented perpendicular to the field will interact less. Time-dependent density functional theory showed that un-terminated σ bonds produce much more emission than the conduction band electrons.[30,31] Figure 2 illustrates two types of initial state densities; a green rectangle represents the de-localized electrons found away from the edge, the density of these states depends linearly on

energy, and the electron concentration is governed by the Fermi distribution. The red oval represents electrons in a single localized edge state; the edge state energy depends on the atomic arrangement but each bond has a single energy.

In addition to simple tunneling, many-body processes can create additional emission at energies higher than the Fermi distribution would predict.[32] When an electron below E_F is emitted, energy is injected into the emission site in the form of a hot hole. If some of that energy is transferred to a single electron originally near E_F, that electron acquires significant energy and so can be emitted with much higher probability. The red and blue arrows illustrate this process in the figure. The emission spectra of metals typically extend several eV above the Fermi energy, which is explained by this mechanism.[33] The probability of emission of the energetic electrons from graphene should be larger than from metals because the scattering rate is lower, and the tunneling probability increases more rapidly with energy than it would for a larger radius structure.

We performed emission characterization inside an ion-pumped stainless steel vacuum chamber equipped with an optical microscope, wire probes, heated specimen stage, residual gas analyzer, and a hemispherical energy analyzer (Scienta-Omicron Argus) mounted with axis 30° above the horizontal sample plane. Prior to testing, we heated the specimen wafers to approximately 200 °C to remove adsorbed water. During testing, the total pressure remained below 10^{-6} Pa and was composed mainly of nitrogen and hydrogen. A pair of Keithley 237 source-measure units applied potentials to and measured current at the gate and drain electrodes relative to the source electrode. Holding the source electrode negative produced vacuum electrons with significant energy relative to the chamber, allowing energy analysis. Positioning a probe a short distance (~100 μm) above the wafer surface provided a means to deflect the emitted beam into the analyzer as well as a means to collect a portion of the emitted beam and verify that emission to vacuum occurred.

Figure 3 shows two sets of emission energy spectra produced by graphene edge diodes made from CVD graphene and RGO. The energies are plotted relative to the Fermi energy of the source contact assuming the analyzer work function φ_a to be 4.65 eV. The emission at energies near the source Fermi energy E_F is excellent confirmation that the electrons were produced by field emission as opposed to thermionic emission, photoemission, or secondary emission since the latter processes produce electrons only at energies greater than the source work function φ_s or above the Fermi energy of the drain electrode plus φ_d.

The emission spectra shown in Fig. 3(a) were produced by a diode specimen made from CVD graphene while the drain-source voltage was held at V_{DS} = 125 V, 135 V, and 145 V. The total emission current averaged roughly 2 pA, 200 pA, and 20 nA, respectively; however, both the current and spectral shape fluctuated during data acquisition. The spectra measured at 135 V and 145 V are plotted after removing a shift of 0.2 eV relative to the 125 V spectrum. All three spectra have linear slopes near E_F that are consistent with emission from a Fermi distribution, indicating the initial states were π states in the graphene conduction band. All three spectra have a slope near E_F that can be fitted using the same elevated temperature (550 K) in the Fermi distribution function, suggesting that the electron temperature is significantly higher than the

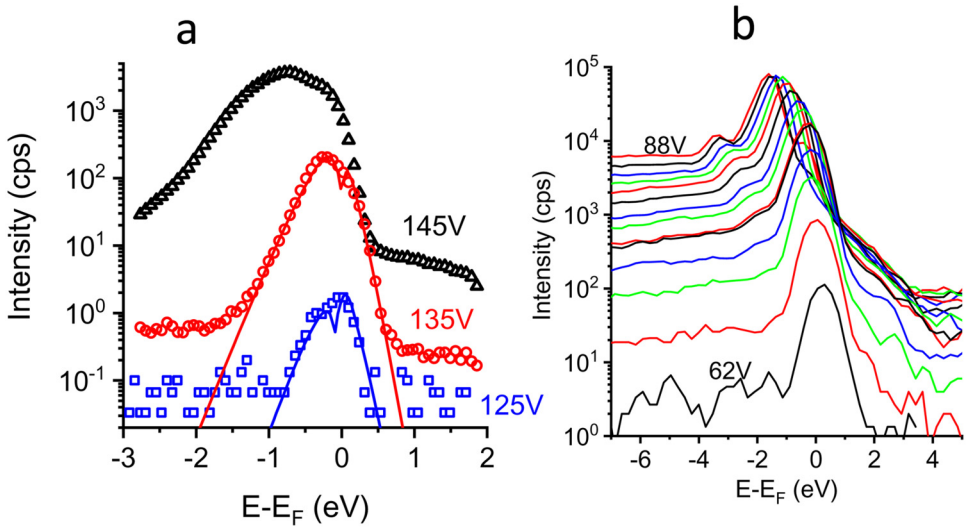

FIG. 3. Field emission energy distributions measured from (a) CVD graphene transferred from copper foil; each curve is labeled with the drain-source voltage applied during the measurement. (b) Reduced graphene oxide; the colored curves are arranged in the sequence black, red, green, and blue as the drain-source voltage increased in 2 V increments, from 62 V to 88 V.

lattice temperature. The emission spectrum did not fit the typical field emission produced by metals, but we could produce good fits to the 125 V and 135 V spectra (solid lines) by multiplying by the graphene density of states. That is $I(E) = A\,D(E)T(E)F(E)$, where $D(E) \propto |E - E_A|$ (the density of delocalized states created by π orbitals where E_A is the accumulation energy $E_A = E_F - E_D$), $T(E) = e^{-E/d}$ (d is proportional to the potential applied across the diode), and $F(E) = (1 + e^{-E/kT})^{-1}$. The electron density at $E = E_A$ is zero; hence, a spectrum calculated using a single value of E_A also goes to zero at $E = E_A$. The solid lines in Fig. 3(a) show calculated spectra where two spectra with different values of E_A have been added, such that the spectrum does not go to zero but contains a sharp dip. This sharp feature does not appear in the data; this is expected because of the broadening caused by factors not considered in the calculation such as the resolution of the analyzer and additional values of E_A (which may be caused by varying state density along the edge and un-intentional chemical doping). If there were no edge states all of the charge would accumulate in the conduction band, such that the Fermi energy would be well above E_D; for example $E_A = 0.5$ eV. However, the 125 V and 135 V spectra could be roughly fit using two values of E_A set to 0.0 eV and 0.1 eV. The small values of E_A indicate that much of the field was terminated by charge in edge states, preventing more accumulation.

The emission distribution measured at 145 V could not be fit in the same way because it contains an additional peak about 1 eV below E_F. This energy is consistent with calculated emission from edge states.[32] The relative intensities of the peak near E_F and the lower energy peak fluctuated during data acquisition. Such fluctuations are consistent with emission from a small number of sites with intermittent termination or coordination. Similar fluctuations were also observed in the I-V characteristics discussed below. The 145 V spectrum also shows significant emission at energies up to at least 1.6 eV above E_F. Assuming that the emission at +1.6 eV is caused by energy released by emission at least 1.6 eV below E_F as shown in Fig. 2, the high energy portion of the spectra confirms that emission from states well below E_F must have occurred. This shows that the low energy emission was not caused by local shifts in E_F, perhaps caused by limited transport to the emission site.

The emission spectra produced by the RGO, shown in Fig. 3(b), was significantly different from the CVD graphene. The spectra were primarily composed of a single relatively symmetric peak, centered near E_F at the lower emission current. The high energy side of the spectrum does not fall off exponentially with energy in a way that matches the Fermi distribution function, as observed from the CVD graphene. The symmetric peak shape is consistent with emission from a single initial state such as an edge bond, as opposed to an energy band filled according to Fermi statistics. The dominance of the symmetric peak may result from the much larger density of defect sites and much smaller grain size known to exist in RGO. A second peak becomes visible at higher emission current, initially at about −1.5 eV. Both peaks shift to lower energy at higher emission current. At the two highest applied voltages ($V_{DS} = 88$ V and 90 V), a third peak appears close to E_F. The third peak might come from an area having a relatively large tunnel barrier, such as where an additional layer of graphene is present. Each of the spectra displayed significant emission extending several eV both above and below E_F. The portion of the spectra significantly below the main peaks can be explained as field emitted electrons re-emitted after losing several eV of energy upon striking another electrode. Similar to the spectra produced by CVD graphene, the emission at energies above E_F can be explained by the transfer of electronic energy generated by emission from states with equal or larger energy below E_F as shown in Fig. 2. This mechanism makes sense here since, in fact, emission at energies at least equally far below E_F and at least an order of magnitude more intense is present in each of the spectra (apart from the electrons detected following energy loss). Again, the emission above E_F shows that much of the low energy emission originated from states several eV below E_F, rather than emission near E_F in local areas where E_F was shifted due to transport effects. Such transport effects do seem to be responsible for the overall shift of the emission spectra toward lower energies at the higher diode voltages and emission current.

Two previous reports on the field emission energy spectra produced by graphene-like material (likely to have multiple layers) showed symmetric peak shapes similar to our measurements of RGO emission. For graphene fabricated by detonation synthesis, the peak position was more than 1 eV below E_F, additional peaks at lower energies were observed, and either or both peaks shifted to lower energies at higher emission current.[34] No emission near or above E_F was reported; however, the dynamic range of the experiment appears to have been too low to show the effect in that work. The emission spectra produced by nano-graphite fabricated via plasma-enhanced CVD showed two peaks, one centered at E_F and one that shifted with emission current, in some cases appearing more than 2 eV below E_F.[35] The two earlier reports do not show a Fermi edge as do the CVD graphene spectra shown in Fig. 3(a).

The difference in the emission spectra produced by the CVD graphene, RGO, and graphene produced in previous work shows that the graphene quality can have a major impact on the emission spectra. The differences in the spectra appear to reflect differences in the density of electrons in the conduction band vs edge states.

IV. VACUUM FIELD EFFECT TRANSISTOR SIMULATION AND MEASUREMENTS

Graphene vacuum field effect transistors (VFETs) can produce significant gain and power at mm-wave frequencies, if sufficient linear current densities are achieved.[1] The planar edge geometry combined with the velocity of electrons in vacuum can result in transit times below 1 ps as well as high maximum voltages and low capacitances. Nearly complete drain current saturation can be achieved by designs that shield the source from the drain using the gate and other electrodes. However, in the present preliminary work, we used a simple design and so drain current saturation is not

achieved. The three-terminal design is employed here primarily as a means to confirm field emission and distinguish vacuum transport from solid state transport.

We measured the drain current as a function of drain-source voltage at different fixed gate-source voltages. Applying more negative voltage to the gate reduced the drain current, consistent with the field emission mechanism. This result rules out significant solid state transport from the gate to the drain since the drain current would increase for more negative gate voltages. We can also compare the measurements with simple theory (i.e., assuming the WKB approximation). According to WKB, $T(E)\ e^{-G}$, where $G = g\sqrt{U(x)}$, where the integral is taken over the range where $U(x)$ is positive, and $g = 2\sqrt{2\,m}/\hbar = 10.24\ \mathrm{eV}^{-1/2}\ \mathrm{nm}^{-1}$. The potential $U(x)$ can be calculated numerically assuming an abrupt interface at the graphene edge. An example calculation is plotted in Fig. 4 assuming the length of the vacuum channel (gap between graphene edges), gate electrode, and trench depth are each 500 nm, $V_{GS} = 0$, and $V_{DS} = 200$ V.[36] The graphene is modeled as a 0.2 nm thick conducting sheet with a semicircular edge having 0.1 nm radius. The electron trajectories in Fig. 4(a) are calculated assuming they start with zero initial energy at points where the vacuum potential is 4.5 eV more positive than at the surface. The model shows that the total charge in the source electrode is 5.7 electrons/nm, the time required for an electron to move 500 nm away from the graphene edge is less than 100 fs, and space charge is negligible for emission current below 10 mA/mm. With $V_{GS} = 0$, the trajectories arc up over the opposite graphene edge and terminate over a relatively large area up to several microns away. Some of the trajectories can be directed upward by applying positive potential to an additional electrode hovering near the device; this allowed measurement of the electron energy distribution. The trajectories move further up and to the right when negative gate voltages are assumed, and bend down toward the recessed substrate when the gate voltage is positive. Figure 4(b) shows calculated potential contours near the graphene source edge. A horizontal line starting at the graphene edge, marked with vertical lines at 1 nm and 2 nm, is shown for reference. Figure 4(c) is a plot of the energy $U(x)$ along the line, assuming an abrupt barrier $\varphi = 4.5$ eV between the emitter Fermi energy and the vacuum level at the graphene-vacuum interface. For comparison, a triangular barrier representing a constant field $F = 3$ V/nm (which is typical of field emission from metal tips), is also plotted. It is clear that in this case the

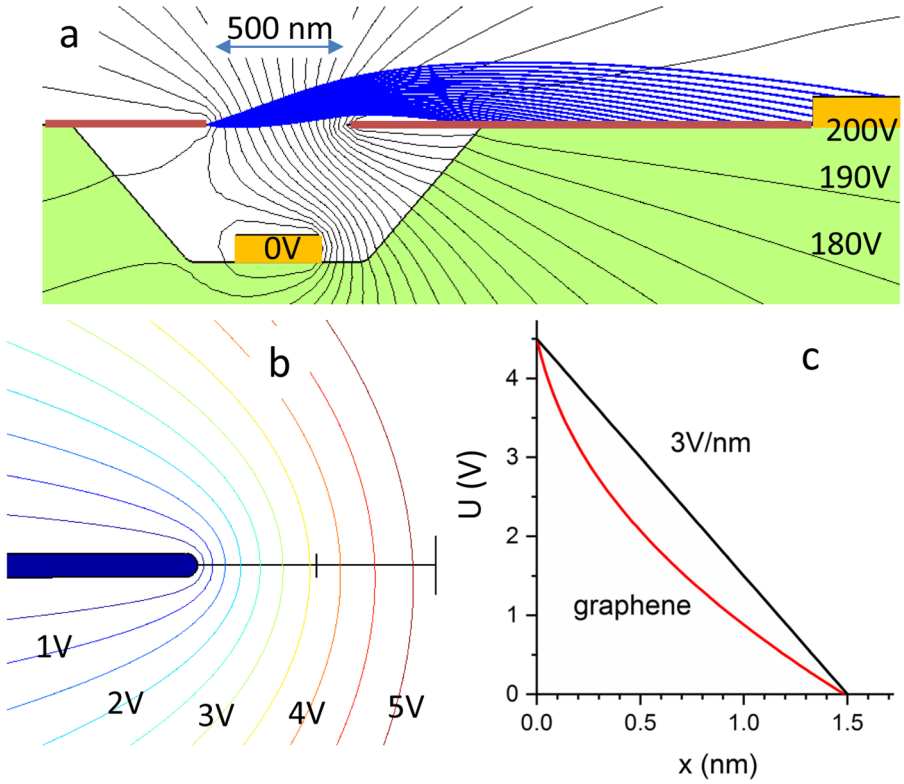

FIG. 4. Results of a numerical solution of the electric potentials near the device electrodes. (a) Potential contours in 10 V increments (black lines) and electron trajectories (blue lines) calculated when the drain (right side horizontal red line) is 200 V and the gate is 0 V with respect to the source (left side horizontal red line). (b) Potential contours in 0.5 V increments near the graphene edge; the horizontal line is marked at 1 and 2 nm. (c) A plot of the potentials along the horizontal line after adding 4.5 V abruptly at the edge. A linear plot is shown for comparison.

tunneling barrier for an electron at the Fermi level of the graphene edge (the square root of the shaded area) is smaller than the triangular barrier. In reality, the interface potential should be less abrupt such that the barrier is reduced to some extent, increasing the tunneling probability.[37] Neglecting the interface correction, the integral of U(x) from Fig. 4(c) results in $T = 1.5 \times 10^{-8}$ when $V_{DS} = 200$ V. The tunneling probability increases by a factor of 350 (to 5.3×10^{-6}) when V_{DS} is increased to 250 V ($V_{GS} = 0$ in both cases). In our measurements, the current increased more quickly with voltage, as discussed below.

The solid lines in Fig. 5 show drain-source I_{DS}-V_{DS} measurements from a gated device made from CVD graphene, with the gate voltage V_{GS} set to 0, −60, −80, and −100 V (held constant during the I_{DS}-V_{DS} measurements). At drain voltages below about 200 V, I_{DS} rose linearly due to current flowing through the external circuit but remained below 10 pA. The current rose rapidly with V_{DS} above threshold voltages that increased with more negative values of V_G. The threshold voltages are consistent with estimates based on the numerical model. The current increased from 12 pA to 8.6 nA as V_{DS} increased from 200 to 250 V, a factor of 720, more than twice the ratio calculated above. Accumulation and/or other reductions in the barrier potential with increased V_{DS} might account for the discrepancy.

Since three electrodes are present, the field at the graphene edge is proportional to a linear combination of the voltages applied between the gate and drain electrodes relative to the source electrode $V_C = V_{DS} + CV_{GS}$, where C is a constant that depends on the geometry of the electrodes. The geometry shown in Fig. 1 produces a value of C close to 1. Replacing V with V_C in Eq. (1), the emission current should change with V_C as $I = AV_C^k e^{\left(\frac{-B}{V_C}\right)}$, where the value of k is not known but may be <2 as discussed previously. The points plotted as open circles in Fig. 1 are calculated assuming $k = 0$, using the least squares method to determine A and B, and adjusting C to produce good fits to both data sets ($V_{GS} = 0$ and −100 V); this process produced C = 0.82.

Figure 6 shows plots of ln(I) vs $1/V_{DS}$ for each of the curves measured at different V_{GS} (open circles). Plotting this way does not assume $k = 2$ as does the traditional Fowler-Nordheim plot. The data are also plotted as ln(I) vs $1/V_C$ (dashed lines). The adjusted data sets fall onto two distinct lines, the two sets measured at $V_{GS} = -60$ and −80 are nearly identical, as are those measured at $V_{GS} = 0$ and −100. Fitting values of A and B yield A = 11.3 and B = −7436 for the former and A = 5.6 and B = −5697 for the latter. All of the plots are linear within experimental error. These measurements do not show that $k = 0$ precisely, since the change in V^k is at most 1.56 (if $k = 2$), whereas the term $e^{\frac{-B}{V_C}}$ changes by factors between 10^2 and 10^3 over the measurement range. Similar measurements over a larger relative voltage range are needed to determine k more precisely.

The plots in Fig. 6 show the emission current fluctuated between two regimes with constant A and B. The individual

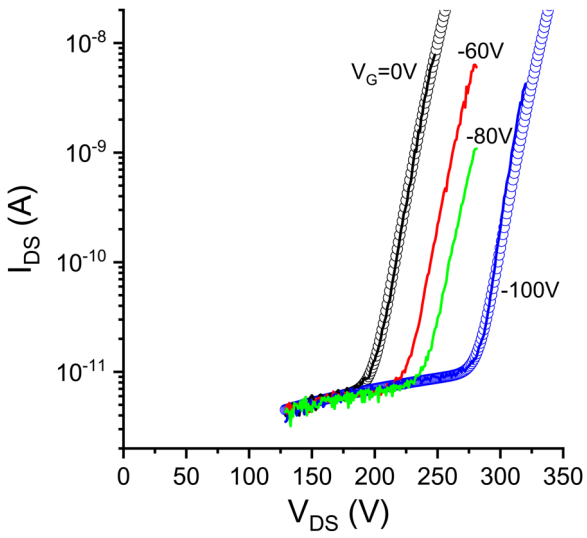

FIG. 5. I-V characteristics of a gated graphene edge field emission transistor measured with gate potential V_{GS} set to 0, −60, −80, and −100 V (solid lines). The open circles show calculated I-V curves using $I_{DS} = Ae^{-\left(\frac{B}{V_C}\right)}$, where $V_C = V_{DS} + CV_{GS}$. The values of *A*, *B*, and *C* have been calculated as *A* = 80821, *B* = 7436, and C = 0.82 by using least squares to fit to the log plots shown in Fig. 6 when $V_G = 0$ and −100 V.

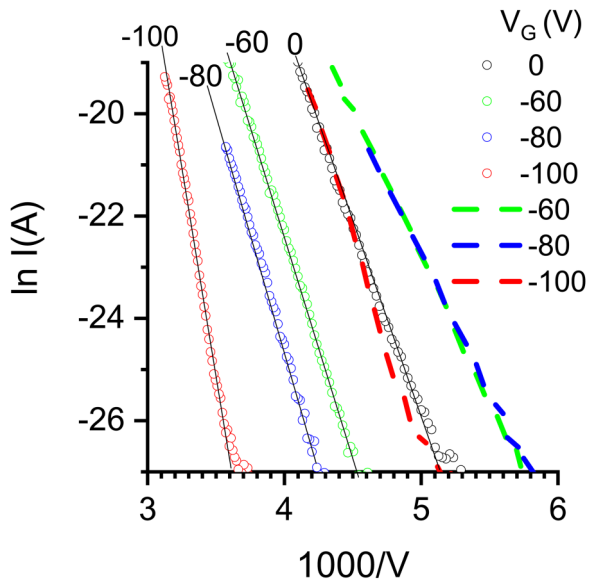

FIG. 6. The same data shown in Fig. 5, plotted as ln(I) vs 1/V (aka Millikan-Lauritsen plots). One curve is plotted for each of the applied gate voltages $V_{GS} = 0$, −60, −80, and −100 V (open symbols). In addition, three data sets are re-plotted as ln(I) vs $1/V_C$, where $V_C = V_{DS} + 0.82V_{GS}$ (dashed lines). The solid straight lines are a guide to the eye. Linear fits to the adjusted data yielded slope and intercept values of −7436 and 11.3 for the lines where $V_{GS} = 0$ and −100 V; and −5697 and 5.6 for the lines where $V_{GS} = -60$ and −80 V.

current measurements made during the automated voltage sweep occurred at roughly 500 ms intervals such that the relevant I-V sweep measurements at a fixed gate voltage occurred within 10 s, but the sets were typically separated by at least 2 min. The current fluctuated spontaneously at intervals long enough that the fluctuations typically did not occur during the 10 s measurement intervals. The fluctuations might be caused by the presence of molecules such as fluorine, hydrogen, or water at or near the emitting edge. Such adsorbate-induced fluctuations would occur only if a significant portion of the emission came from a section of the edge short enough to be affected by a single molecule. The molecules might be removed by the local temperature and/or electronic energy released by emission from below E_F. Molecules bound to the graphene surface with weak Van der Walls forces could be induced to move toward the edge when an electric field is present. This process could supply additional molecules to the edge and account for the observed fluctuation. We did not heat the CVD graphene specimen aggressively in UHV prior to testing in order to prevent damage; using higher temperatures and longer outgassing periods might reduce the fluctuations.

V. SUMMARY

We have demonstrated field emission from planar graphene edges with integrated gate and drain electrodes. The field emission mechanism is proven because the energy of the vacuum electrons is generally near or slightly below the Fermi energy. The energy distributions produced by CVD graphene and RGO are different. Modeling the energy distributions produced by CVD graphene indicates the conduction band was lightly accumulated and that emission came from a combination of both the delocalized π band and local σ edge states. In contrast, the RGO spectra indicate most of the emission comes from local edge states. Gate modulation of the edge field and emission current using an integrated three-terminal design is demonstrated for the first time. The emission current is exponential with V_C from 1 pA to 10 nA. The gate and drain electrode voltages needed to cause field emission from the source are consistent with estimates based on a numerical model of the device. The rate of change of the emission current is about twice as high as the calculation predicted.

ACKNOWLEDGMENTS

This work was supported by the Office of Naval Research. The authors thank Doewon Park for fabrication advice and Dr. Baruch Levush for support and encouragement.

REFERENCES

[1]J. L. Shaw, J. G. Champlain, B. D. Kong, K. L. Jensen, and J. B. Boos, in 2016 *International Vacuum Nano-electronics Conference*, *Vancouver, British Columbia, Canada, 11-15 July 2016* (IEEE XPlore 2016).
[2]K. A. Dean, T. P. Burgin, and B. R. Chalamala, Appl. Phys. Lett. **79**, 1873 (2001).
[3]S. T. Purcell, P. Vincent, C. Journet, and V. T. Binh, Phys. Rev. Lett. **88**, 105502 (2002).
[4]*Vacuum Microelectronics*, edited by W. Zhu (Wiley, 2001).
[5]P. Zhang, L. Ma, F. Fan, Z. Zeng, C. Peng, P. E. Loya, Z. Liu, Y. Gong, J. Zhang, X. Zhang, P. M. Ajayan, T. Zhu, and J. Lou, Nat. Commun. **5**, 3782 (2014).
[6]J. Wang, M. Zhu, X. Zhao, R. Outlaw, D. M. Manos, B. C. Holloway, C. Park, T. Anderson, and V. Mammana, J. Vac. Sci. Technol. B **22**, 1269 (2004).
[7]Z. Xiao, J. She, S. Deng, Z. Tang, Z. Li, J. Lu, N. Xu, ACS Nano **4**, 6332–6336 (2010).
[8]V. I. Kleshcha, D. A. Bandurin, A. S. Orekhova, S. T. Purcell, and A. N. Obraztsova, Appl. Surf. Sci. **357**, 1967 (2015).
[9]S. Santandrea, F. Giubileo, V. Grossi, S. Santucci, M. Passacantando, T. Schroeder, G. Lupina, and A. Di Bartolomeo, Appl. Phys. Lett. **98**, 163109 (2011).
[10]F. Giubileo, A. Di Bartolomeo, L. Iemmo, L. G. Luongo, and F. Urban, Appl. Sci. Basel **8**, 526 (2018).
[11]S. Kumar, G. S. Duesberg, R. Pratap, S. Raghavan, Appl. Phys. Lett. **105**, 103107 (2014).
[12]A. Di Bartolomeo, F. Giubileo, L. Iemmo, F. Romeo, S. Russo, S. Unal, M. Passacantando, V. Grossi, A. M. Cucolo, Appl. Phys. Lett. **109**, 023510 (2016).
[13]P. Blake, E. W. Hill, A. H. Castro Neto, K. S. Novoselov, D. Jiang, R. Yang, T. J. Booth, and A. K. Geim, Appl. Phys. Lett. **91**, 063124 (2007).
[14]H. Schroeder, J. Appl. Phys. **117**, 215103 (2015).
[15]R. Forbes, Appl. Phys. Lett. **92**, 19305 (2008).
[16]R. Forbes, J. Appl. Phys. **105**, 114313 (2009).
[17]K. L. Jensen, D. A. Shiffler, J. R. Harris, I. M. Rittersdorf, and J. J. Petillo, J. Vac. Sci. Technol. B **35**, 02C101 (2017).
[18]A. Kyritsakis and J. P. Xanthakis, Proc. R. Soc. A **471**, 20140811.
[19]A. Modinos, Surf. Sci. **42**, 205 (1974).
[20]Q.-A. Huang, M. Qin, B. Zhang, and J. K. O. Sin, J. Appl. Phys. **81**, 7589 (1997).
[21]Y. S. Ang, M. Zubair, K. J. A. Ooi, and L. K. Ang, e-print arXiv:1711.05898 (2017), and references therein.
[22]F. Urban, M. Passacantando, F. Giubileo, L. Iemmo, and A. Di Bartolomeo, Nanomaterials **8**, 151 (2018).
[23]A. Di Bartolomeo, F. Urban, M. Passacantando, N. McEvoy, L. Peters, L. Iemmo, G. Luongo, F. Romeo, and F. Giubileo, e-print arXiv:1808.02127.
[24]X. Li, W. Cai, J. An, S. Kim, J. Nah, D. Yang, R. Piner, A. Velamakanni, I. Jung, E. Tutuc, S. K. Banerjee, L. Colombo, and R. S. Ruoff, Science **324**, 1312–1314 (2009).
[25]X. Li, C. W. Magnuson, A. Venugopal, R. M. Tromp, J. B. Hannon, E. M. Vogel, L. Colombo, and R. S. Ruoff, J. Am. Chem. Soc. **133**, 2816–2819 (2011).
[26]G. G. Jernigan, J. A. Nolde, N. A. Mahadik, E. R. Cleveland, J. E. Boercker, M. B. Katz, J. T. Robinson, and E. H. Aifer, J. Appl. Phys. **122**, 075301 (2017).
[27]W. Z. Schottky, Physik **14**, 63 (1923).
[28]J. L. Ladoa, N. García-Martínez, and J. Fernández-Rossier, Synth. Met. **210**, 56–67 (2015).
[29]W. Wang, X. Qin, N. Xu, and Z. Li, J. Appl. Phys. **109**, 044304 (2011).
[30]M. Araidai, Y. Nakamura, and K. Watanabe, Phys. Rev. B **70**, 245410 (2004).
[31]K. Tada and K. Watanabe, Phys. Rev. Lett. **88**, 127601 (2002).
[32]J. W. Gadzuk and E. W. Plummer, Rev. Mod. Phys. **45**, 1973.
[33]J. W. Gadzuk and E. W. Plummer, Phys. Rev. Lett. **26**, 92–95 (1971).
[34]G. N. Fursey, N. V. Egorov, I. I. Zakirova, A. M. Yafyasov, L. I. Antonova, and V. V. Trofimov, Comm. Technol. Electron. **61**, 72–75 (2016).
[35]D. A. Bandurin, S. Mingels, V. I. Kleshch, D. Lützenkirchen-Hecht, G. Müller, and A. N. Obraztsov, Appl. Phys. Lett. **106**, 233112 (2015).
[36]Lorentz 2E software (Integrated Engineering Software) used for this calculation.
[37]R. G. Forbes, J. Appl. Phys. **103**, 114911 (2008).